Anomalous Cage Effect of the Excited State Dynamics of Catechol in the 18C6-Catecol Host-Guest Complex.

ARTICLE *in* THE JOURNAL OF PHYSICAL CHEMISTRY B · OCTOBER 2014

Impact Factor: 3.3 · DOI: 10.1021/jp508619f · Source: PubMed

5 AUTHORS, INCLUDING:

Yoshiya Inokuchi
Hiroshima University
94 PUBLICATIONS **1,016** CITATIONS
SEE PROFILE

Takeharu Haino
Hiroshima University
142 PUBLICATIONS **2,548** CITATIONS
SEE PROFILE

Takayuki Ebata
Hiroshima University
209 PUBLICATIONS **5,222** CITATIONS
SEE PROFILE

THE JOURNAL OF PHYSICAL CHEMISTRY B

Article

pubs.acs.org/JPCB

Anomalous Cage Effect of the Excited State Dynamics of Catechol in the 18-Crown-6−Catechol Host−Guest Complex

Fumiya Morishima, Ryoji Kusaka, Yoshiya Inokuchi, Takeharu Haino, and Takayuki Ebata*

Department of Chemistry, Graduate School of Science, Hiroshima University, Higashi-Hiroshima 739-8526, Japan

Supporting Information

ABSTRACT: We determined the number of isomers and their structures for the 18-crown-6 (18C6)−catechol host−guest complex, and examined the effect of the complex formation on the S_1 ($^1\pi\pi^*$) dynamics of catechol under a supersonically cooled gas phase condition and in cyclohexane solution at room temperature. In the gas phase experiment, UV−UV hole-burning spectra of the 18C6−catechol 1:1 complex indicate that there are three stable isomers. For bare catechol, it has been reported that two adjacent OH groups have an intramolecular hydrogen (H) bond. The IR−UV double resonance spectra show two types of isomers in the 18C6−catechol 1:1 complex; one of the three 18C6−catechol 1:1 isomers has the intramolecular H-bond between the two OH groups, while in the other two isomers the intramolecular H-bond is broken and the two OH groups are H-bonded to oxygen atoms of 18C6. The complex formation with 18C6 substantially elongates the S_1 lifetime from 7 ps for bare catechol and 2.0 ns for the catechol−H_2O complex to 10.3 ns for the 18C6−catechol 1:1 complex. Density functional theory calculations of the 18C6−catechol 1:1 complex suggest that this elongation is attributed to a larger energy gap between the S_1 ($^1\pi\pi^*$) and $^1\pi\sigma^*$ states than that of bare catechol or the catechol−H_2O complex. In cyclohexane solution, the enhancement of the fluorescence intensity of catechol was found by adding 18C6, due to the formation of the 18C6−catechol complex in solution, and the complex has a longer S_1 lifetime than that of catechol monomer. From the concentration dependence of the fluorescence intensity, we estimated the equilibrium constant K for the 18C6 + catechol ⇄ 18C6−catechol reaction. The obtained value (log K = 2.3) in cyclohexane is comparable to those for alkali metal ions or other molecular ions, indicating that 18C6 efficiently captures catechol in solution. Therefore, 18C6 can be used as a sensitive sensor of catechol derivatives in solution with its high ability of fluorescence enhancement.

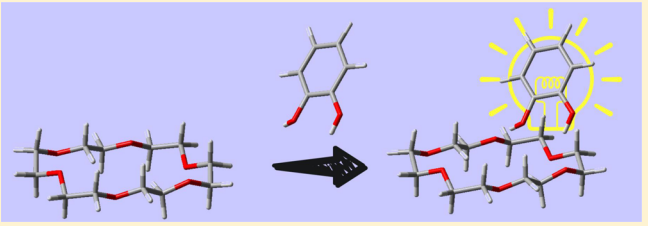

1. INTRODUCTION

Catechol (1,2-dihydroxybenzene) has two OH groups forming an intramolecular hydrogen (H) bond (see Scheme 1). The structure of catechol and its complexes in the electronic ground (S_0) and excited (S_1) states has been investigated extensively in the gas phase.[1−8] The catechol monomer has C_s symmetry in the S_0 state. In the S_1 state, the free OH group is twisted out of plane of the benzene ring, and the symmetry of catechol is reduced to C_1.[2,3,5] The electronic excited state dynamics of catechol has also been investigated extensively by many researchers;[9−12] catechol has a rather short S_1 lifetime (7−12 ps) compared to other similar aromatic molecules such as phenol (2 ns), 1,3-dihydroxybenzene (resorcinol) (>1 ns), and 1,4-dihydroxybenzene (hydroquinone) (0.43 ns).[9−14] This very short lifetime of catechol is explained by a nonradiative mechanism similar to phenol. Phenol O−H bond fission undergoes thorough H atom tunneling from the optically allowed S_1 ($^1\pi\pi^*$) to the repulsive S_2 ($^1\pi\sigma^*$) state below the S_1/S_2 conical intersection, and finally produces an H atom and a phenoxy radical.[15−22] Catechol also relaxes through a similar route and releases an H atom from the ^{b}OH group (see

Scheme 1. Structures of 18-Crown-6 (18C6) and Catechol Monomer with Classification of Two OH Groups[a]

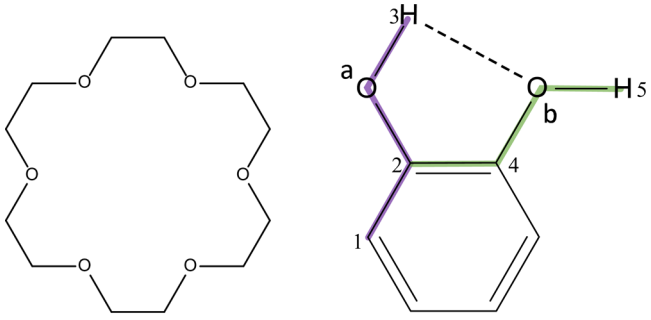

18C6 catechol

[a]The dashed line represents an intramolecular H-bond (^{a}O−H···^{b}O). The purple and green lines exhibit two dihedral angles related to the OH groups, C1−C2−^{a}O−H3 and C2−C4−^{b}O−H5, respectively.

Special Issue: Photoinduced Proton Transfer in Chemistry and Biology Symposium

Received: August 26, 2014
Revised: October 26, 2014

   dx.doi.org/10.1021/jp508619f | J. Phys. Chem. B XXXX, XXX, XXX−XXX

Scheme 1).[10,11] The crucial difference between catechol and phenol is a smaller energy gap between the $^1\pi\pi^*$ and $^1\pi\sigma^*$ states for catechol due to the intramolecular H-bond.[9] In addition, the symmetry of catechol is lowered to C_1 in the S_1 state. The smaller energy gap and the lower symmetry lead to an anomalously fast nonradiative decay from $^1\pi\pi^*$ to $^1\pi\sigma^*$ for catechol.

In the present study, we investigated the structure of the 18-crown-6 (18C6)−catechol host−guest complex and the effect of the complex formation on the S_1 dynamics of catechol. 18C6 is a well-known host species in host−guest chemistry (see Scheme 1). In our previous study, we investigated the structure of cold 3*n*C*n*−phenol complexes (n = 5−8) in supersonic free jets and found that the 18C6−phenol complex forms a single unique isomer, while other complexes with different sizes of crown ethers form several isomers even under the supersonically cooled condition.[23] The observation of the single isomer for the 18C6−phenol host−guest complex was described by the fact that phenol is inserted into the 18C6 cavity like a "lock and key" in this complex and the structure is largely stabilized through collective intermolecular interactions. Here, we extended that work to the 18C6−catechol complex. In bare catechol, the two OH groups form an intramolecular H-bond (intra-H-bond) (Scheme 1). This intra-H-bond may be broken in the 18C6−catechol due to the formation of an intermolecular H-bond (inter-H-bond) with the ether oxygen(s) of 18C6. The complex formation will affect the photophysics of catechol. In this study, bare catechol and its 18C6 complexes are generated under jet cooled conditions utilizing a molecular beam approach. Several laser spectroscopic methods are applied to measure electronic and IR spectra in the gas phase. Complex structures were determined from the observed and calculated IR spectra. The S_1 lifetime of the 18C6−catechol complex was obtained by deconvolution of fluorescence decay profiles. In addition, we measured the S_1 lifetime of the catechol monomer and catechol−H_2O complex by picosecond pump−probe spectroscopy. We will discuss how the complex formation with 18C6 affects the conformation of catechol and its S_1 state dynamics. In addition to the gas phase study, we also investigated the complex formation in cyclohexane solution. We observed the anomalous increase of the fluorescence quantum yield of catechol in cyclohexane solution by the addition of 18C6. From the concentration dependence of the fluorescence intensity, we estimated the equilibrium constant for the complex formation between 18C6 and catechol in cyclohexane, which will give insight into the ability of 18C6 to act as a highly sensitive catechol sensor in solution.

2. EXPERIMENTAL AND COMPUTATIONAL

2.1. Gas Phase Experiment. Details of the experimental setup have been described elsewhere.[24] Jet-cooled catechol and the 18C6−catechol complex were generated by employing the supersonic expansion of a gaseous mixture of 18C6 and catechol with He carrier gas. 18C6 and catechol, which are solid at room temperature, were independently heated to be vaporized in different sample housings, and the 18C6/catechol gas mixture diluted with He carrier gas at a total pressure of 3−4 bar was expanded to a vacuum chamber through a 1 mm orifice of a pulsed nozzle. We applied laser-induced fluorescence (LIF) spectroscopy to obtain the S_1−S_0 electronic spectra. A tunable UV light obtained by second harmonics generation (SHG) of an output of the Nd^{3+}:YAG laser pumped dye laser (Lambda Physik Scanmate/Continuum Surelite II) was introduced into the vacuum chamber to be crossed with the supersonic jet at ∼30 mm downstream of the orifice. LIF spectra were obtained by detecting the total fluorescence as a function of the UV frequency. We also performed UV−UV hole-burning (HB) spectroscopy[25] to discriminate peaks belonging to different isomers; the frequency of the probe UV laser was fixed to a certain vibronic band of a specific species, and its fluorescence intensity was monitored. Under this condition, another tunable UV laser (pump laser) pulse obtained by SHG of the Nd^{3+}:YAG laser pumped dye laser (Continuum ND6000/Surelite II) was introduced 10 mm upstream of the crossing point between the jet and the probe laser with ∼4 μs prior to the probe laser pulse. The frequency of the UV hole laser was scanned, and depletion of the fluorescence intensity induced by the absorption of the pump laser was observed. Thus, the UV−UV HB spectra were obtained as fluorescence-dip spectra. For IR−UV double resonance (DR) spectroscopy, the output of a pulsed tunable IR laser (Laser Vision/Quanta-Ray GCR250) was employed as a pump laser. The IR laser was introduced coaxially to the probe UV pulse with an interval of 80 ns prior to the UV pulse. The UV probe laser frequency was fixed to a certain vibronic band, and the IR laser frequency was scanned. A depletion of the fluorescence induced by the IR pump laser was detected, giving fluorescence-dip IR spectra for the UV monitored species.

The S_1 lifetime of the 18C6−catechol complex was obtained by deconvoluting the time profiles of the fluorescence decay curve by assuming the laser pulse could be described by a Gaussian function with 5.0 ns pulse width. In addition, we measured the S_1 lifetime of catechol and the catechol−H_2O complex by pump−probe experiment with a picosecond laser system. In this experiment, the molecule or complex in the molecular beam is ionized by stepwise two-photon ionization with two picosecond lasers. The first picosecond pump pulse photoexcites the molecule to the S_1 origin, and the second probe laser pulse photoionizes the S_1 state molecule to the ionic state (D_0). By changing the delay time between the pump and probe lasers, we obtain the decay time profile of the S_1 state. The setup of the picosecond laser system has also been described in detail elsewhere.[26,27] The two tunable picosecond UV laser pulses were obtained by SHG of two optical parametric generation/optical parametric amplifier (OPG/OPA) systems (Ekspla PG401 SH) pumped by a mode-locked picosecond Nd^{3+}:YAG laser (Ekspla PL2143S). The spectral and time resolution of the two UV pulses were 5 cm^{-1} and 12 ps, respectively. The two lasers (pump and probe) are introduced to a molecular beam machine, and crossed with the molecular beam in a counter-propagated manner with each other. The delay time between the pump UV and probe UV laser pulses was controlled with an optical delay line. The ions were mass-analyzed with a 50 cm time-of-flight tube and were detected by a channeltron (Burle 4900). The ion signals were processed by a boxcar integrator (Par model 4401/4420) connected with a PC. The decay time constants were obtained by a convolution method. All the decay curves could be fitted as a single exponential decay. 18C6 and catechol were purchased from Sigma-Aldrich and NACALAI TESQUE, respectively, and used without further purification.

2.2. Liquid Phase Experiment. The UV absorption spectra of pure catechol and the catechol/18C6 mixture were measured in cyclohexane solution with a commercial spectrophotometer (Hitachi U-3010). Fluorescence spectra were observed for the catechol/18C6 mixture in cyclohexane solution with a fluorescence spectrophotometer (Hitachi F-2500), by changing the concentration ratio of catechol:18C6 from 1:0 to 1:9, where the concentration of catechol was fixed at 1.0×10^{-4} mol/L. This

dx.doi.org/10.1021/jp508619f | J. Phys. Chem. B XXXX, XXX, XXX−XXX

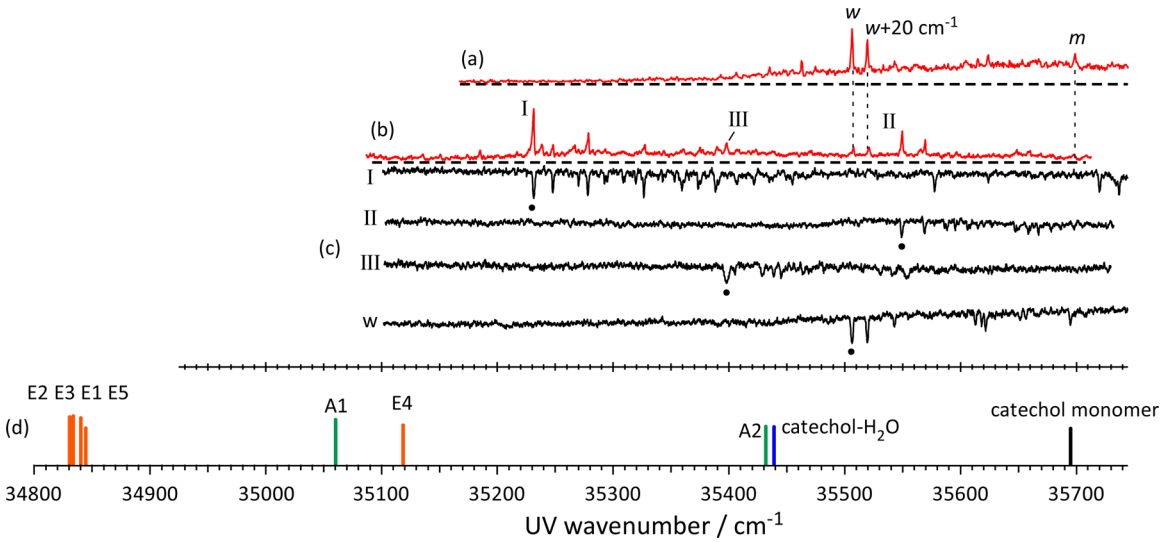

Figure 1. (a) The S_1-S_0 LIF spectrum of catechol in a supersonic free jet. Bands ***m*** and ***w*** are assigned to catechol monomer and catechol−H_2O 1:1 complex, respectively. (b) The S_1-S_0 LIF spectrum of 18C6−catechol in a supersonic free jet. Bands **I**, **II**, and **III** are attributed to different isomers of the 18C6−catechol complex. (c) UV−UV HB spectra of 18C6−catechol (**I**−**III**) and H_2O−catechol complex. These spectra are observed by monitoring the fluorescence intensity of the origin bands, which are labeled with solid circles. (d) The position of the S_1-S_0 transitions obtained with TD-DFT calculation for catechol monomer (black), catechol−H_2O complex (blue), and 18C6−catechol complexes (green for **A1** and **A2** and orange for **E1**−**E5**). The calculations were carried out at the ωB97X-D/6-31++G** level. The transition energies are displayed in eV in Table 2.

low concentration ensures no self-aggregation of catechol in cyclohexane. In addition, we measured the fluorescence lifetime of catechol and the 18C6−catechol mixture in cyclohexane solution by using a HORIBA Tem Pro1. The diode laser used for the excitation emits 250 nm light with a pulse width of 1.2 ns.

2.3. Computational. To obtain plausible structures of the 18C6−catechol complex, we first used a classical force field to search initial conformations. We performed a Monte Carlo simulation by mixed torsional search with low-mode sampling[28] in MacroModel V.9.1[29] with the MMFF94s force field,[30] and optimized the geometries by the PRCG algorithm with a convergence threshold of 0.05 kJ/mol. From this calculation, 193 isomers for the 18C6−catechol complex were obtained within 20 kJ/mol of the most stable one. All of these isomers were geometry-optimized by density functional theory (DFT) calculations at the M05-2X/6-31+G* level with *loose* optimization criteria. Then, 61 isomers were obtained within 20 kJ/mol. These 61 isomers were further optimized at the ωB97X-D/6-31++G** level with *tight* optimization criteria and an *ultrafine* grid. To obtain calculated IR spectra and electronic transition energies, we performed vibrational analysis and TD-DFT calculations at the ωB97X-D/6-31++G** level. All DFT calculations were performed with the Gaussian 09 package, revision D.01.[31] The OH stretching frequencies and electronic transition energies are scaled by 0.9325 and 0.8598, respectively, to reproduce the observed OH stretching vibration frequencies and the S_1-S_0 vertical transition energy of catechol monomer.

3. RESULTS

3.1. Gas Phase Experiment. Figure 1a shows the LIF spectrum of jet-cooled catechol in the S_1-S_0 band origin region without adding 18C6. Band ***m*** at 35695 cm^{-1} is assigned to the (0, 0) band of catechol monomer and band ***w*** at 35506 cm^{-1} to the catechol−H_2O 1:1 complex.[3] The appearance of the catechol−H_2O complex is due to residual water in solid catechol. The intensity of band ***m*** is very weak in the LIF spectrum because of the low fluorescence quantum yield due to the short S_1 lifetime of catechol,[12] while band ***w*** of the catechol−H_2O complex appears much stronger. The band located at 20 cm^{-1} higher frequency of band ***w*** is a vibronic band of catechol−H_2O. Figure 1b shows the LIF spectrum measured by expanding the 18C6/catechol vapor mixture. The bands in the 35200−35600 cm^{-1} region can be assigned to the 18C6−catechol 1:1 complex. Figure 1c shows the UV−UV HB spectra measured by monitoring bands **I**, **II**, **III**, and ***w***. These results indicate that bands **I** (35230 cm^{-1}), **II** (35548 cm^{-1}), and **III** (35397 cm^{-1}) belong to different 18C6−catechol isomers. Similar to the catechol−H_2O complex, the bands of the 18C6−catechol complex are much stronger than the monomer band. Hereafter, we call these isomers, showing bands **I**, **II**, and **III**, isomers **I**, **II**, and **III**, respectively.

Parts b−d of Figure 2 display the IR−UV DR spectra in the OH stretching region measured by monitoring the fluorescence intensity at bands **I**−**III**. Table 1 lists the observed frequencies of the OH stretching vibrations for catechol, catechol−H_2O, and 18C6−catechol. The IR spectrum of catechol monomer (band ***m***) could not be measured because of the weak LIF intensity. Thus, we reproduced the IR spectrum of catechol as a stick diagram (Figure 2a) by using the positions and relative intensities reported by Gerhards et al.[6] The IR bands of bare catechol at 3611 and 3673 cm^{-1} are assigned to the stretching vibration of the donor (^{a}O−H) and acceptor (^{b}O−H) OH groups, respectively.[6] The OH stretching bands of isomers **I** and **II** (Figure 2b and c) appear in the 3350−3450 cm^{-1} region. The IR spectrum of band **I** (Figure 2b) shows two OH stretching bands at 3385 and 3407 cm^{-1}. The IR spectrum of band **II** (Figure 2c) gives only one band at 3424 cm^{-1}. No band is seen in the 3600−3700 cm^{-1} region of bands **I** and **II**, indicating no free OH group in the 18C6−catechol complexes. In addition, isomers **I** and **II** do not have the intra-H-bond between the two OH groups, because they do not show the stretching vibration assignable to the intra-H-bonded OH group in the 3500−3600 cm^{-1} region; the intra-H-bonded OH stretch of catechol−H_2O was observed at 3597 cm^{-1}.[6] Hence, we concluded that in isomers **I** and **II**

dx.doi.org/10.1021/jp508619f | J. Phys. Chem. B XXXX, XXX, XXX−XXX

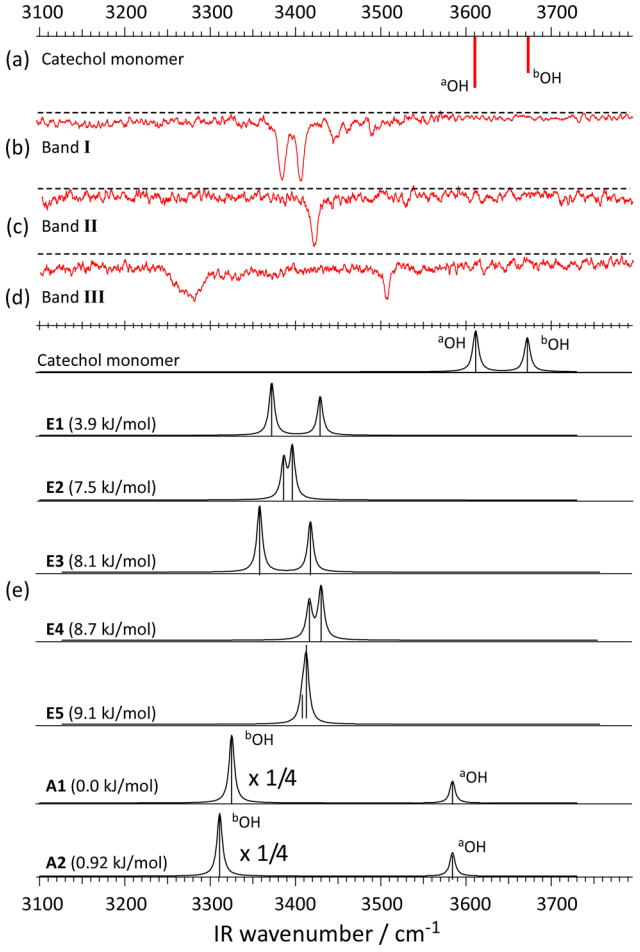

Figure 2. (a) The IR spectrum of bare catechol in the gas phase. The spectrum is shown as a stick diagram by using the positions and relative intensities reported by Gerhards et al. (ref 6). (b–d) The observed IR–UV DR spectra of 18C6–catechol for bands **I**, **II**, and **III**, respectively. (e) The IR spectra of isomers **A1**, **A2**, and **E1**–**E5** of the 18C6–catechol complex obtained by the DFT calculation at the ωB97X-D/6-31++G** calculation level. The calculated frequencies are shown in Table 2.

both of the two OH groups are H-bonded to oxygen atoms of 18C6. The reason for the appearance of only one OH stretch band for isomer **II** (Figure 2c) is probably due to the overlap of the two OH bands, as will be described later. Isomer **III** has two OH bands at 3281 and 3507 cm^{-1}. The band at 3281 cm^{-1} is the stretching vibration of the ^{b}OH group, which is H-bonded to the oxygen atom of 18C6. The band at 3507 cm^{-1} is ascribed to the stretching vibration of the ^{a}OH group having the intra-H-bond with the ^{b}OH group.

The lifetime of catechol in the gas phase at the S_1 origin was reported as 7.0–8.7 ps.[11,12] In the present study, we measured the S_1 lifetime of bare catechol, catechol–H_2O 1:1 complex, and 18C6–catechol 1:1 complex; these results are displayed in Table 1. The results obtained by picosecond pump–probe experiments for catechol and catechol–H_2O 1:1 complex are displayed in Figure 3a. By fitting the time profiles with a single

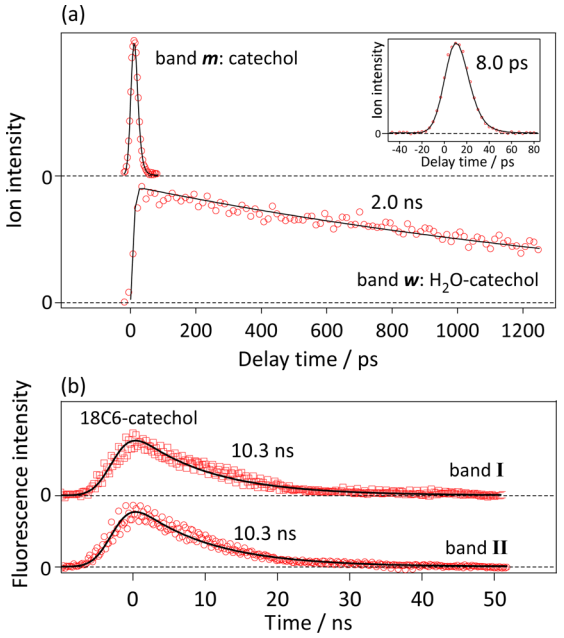

Figure 3. (a) Pump–probe decay profile of bare catechol (band ***m***) and H_2O–catechol (1:1) complex (band ***w***). The inset window displays an expanded view of the time profile of the bare monomer. (b) Fluorescence decay curves measured at bands **I** and **II** of the 18C6–catechol complex.

exponential decay, the S_1 lifetime of catechol at the S_1 band origin was estimated to be 8.0 ps, which is consistent with the reported values.[11,12] The S_1 lifetime of catechol–H_2O is obtained to be 2.0 ns; the formation of an inter-H-bond for the ^{b}OH group elongates the S_1 lifetime of catechol, similar to the case of phenol.[14] For the 18C6–catechol 1:1 complex, we obtained the S_1 lifetime from the fluorescence decay curve at bands **I** and **II** (Figure 3b). Deconvolution of the decay profiles with the laser pulse width of 5.0 ns and by assuming a single exponential decay gives the fluorescence lifetime of bands **I** and **II** to be 10.3 ns for both species; band **III** is too weak for the time profile to be measured with a good signal-to-noise ratio like that in Figure 3b, but its time constant is thought to be comparable to those of

Table 1. Observed Frequencies of the OH Stretching Vibration, Positions of the Origin Band of the S_1–S_0 Transition, Lifetime of Catechol, Catechol–H_2O, and 18C6–Catechol (isomers I–III) at the S_1 Origin Band, and the Structure Assignment of 18C6–Catechol (Isomers I–III)

	OH stretching freq (cm^{-1})	S_1–S_0 transition energy (cm^{-1})	S_1 lifetime	structure
bare catechol	3611 (^{a}OH),[a] 3673 (^{b}OH)[a]	35695	8 ps	
catechol–H_2O	3597 (^{a}OH),[a] 3499 (^{b}OH)[a]	35506	2.0 ns	
isomer **I**	3385, 3407	35230	10.3 ns	E1
isomer **II**	3424	35548	10.3 ns	E4
isomer **III**	3507 (^{a}OH), 3281 (^{b}OH)	35397		A1

[a]Reference 3.

dx.doi.org/10.1021/jp508619f | J. Phys. Chem. B XXXX, XXX, XXX–XXX

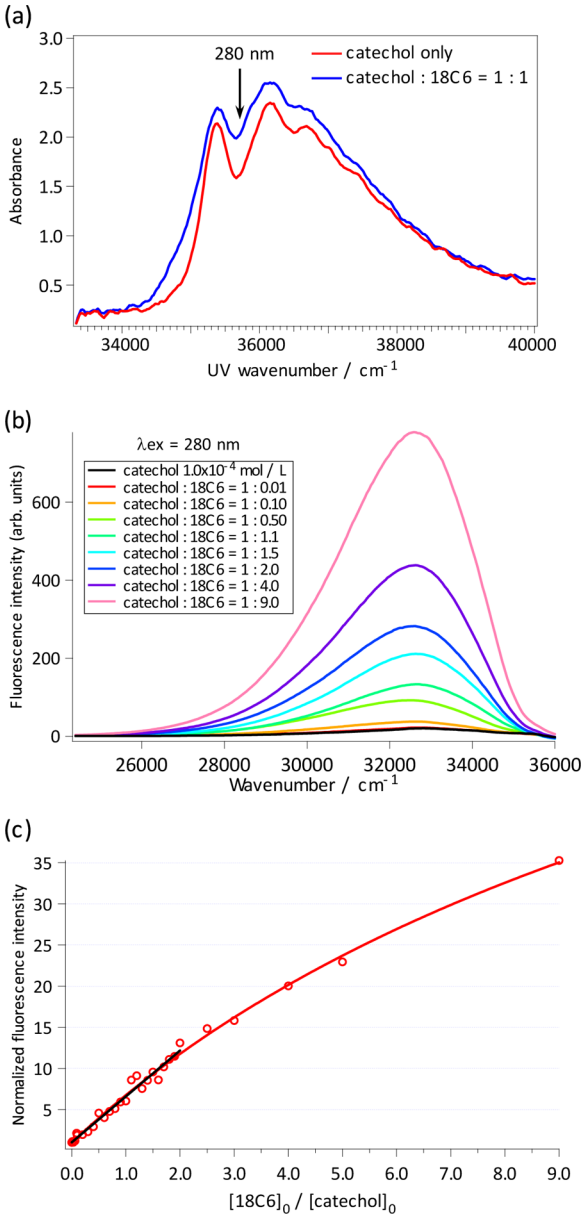

Figure 4. (a) The UV absorption spectra of catechol (red) and 18C6/catechol mixture (blue) in cyclohexane solution. In both solutions, the concentration of catechol was $[18C6]_0 = 5.3 \times 10^{-4}$ mol/L. (b) The UV fluorescence spectra of catechol at different $[18C6]_0/[catechol]_0$ concentration ratios in cyclohexane solution. The excitation wavelength for these spectra was 280 nm (35714 cm^{-1}). $[18C6]_0 = 1.0 \times 10^{-4}$ mol/L for all of the spectra. (c) The integrated fluorescence intensity of catechol as a function of the $[18C6]_0/[catechol]_0$ concentration ratio. The intensities are normalized with respect to the fluorescence intensity of pure catechol. The black line represents the linear fit in the range $0 < [18C6]_0/[catechol]_0 < 2.0$. The red curve represents the fitting used by a Hill equation.

bands **I** and **II**. The S_1 lifetime of the 18C6−catechol complex is ∼5 times longer than that of the catechol−H_2O 1:1 complex.

3.2. Liquid Phase Experiment. *3.2.1. Absorption and Fluorescence Spectra.* Figure 4a shows the UV absorption spectra of catechol (red) and 1:1 mixture of catechol and 18C6 (blue) in cyclohexane with a catechol concentration of 5.3×10^{-4} mol/L at room temperature. The blue spectrum has a noticeable gain in the absorption in the 34000−35000 cm^{-1} region. This trend is consistent with the red shift of the (0, 0) band of the 18C6−catechol 1:1 complex with respect to the catechol monomer in the gas phase, as seen in Figure 1. Therefore, the results of the absorption spectra in Figure 4a suggest the formation of the 18C6−catechol 1:1 complex also in cyclohexane solution.

Figure 4b exhibits fluorescence spectra of catechol and catechol/18C6 mixture measured by the UV excitation at 280 nm (35700 cm^{-1}) at room temperature. The catechol concentration was fixed at $[catechol]_0 = 1.0 \times 10^{-4}$ mol/L, and the concentration ratio $[18C6]_0/[catechol]_0$ was increased from 0.0 to 9.0, where $[catechol]_0$ and $[18C6]_0$ are the initial concentrations of catechol and 18C6, respectively. Since 18C6 does not fluoresce in this region, the fluorescence in Figure 4b is due to catechol in solution. The fluorescence intensity increases with increasing concentration of 18C6. This is because the 18C6−catechol 1:1 complex is formed in solution. The band shape in Figure 4b is almost the same for all the 18C6 concentrations. The fluorescence spectrometer used for the fluorescence spectra in Figure 4b does not have a resolution sufficient to detect the fluorescence of the 18C6−catechol complex separately from that of catechol monomer in solution.

Figure 4c shows the plot of the total fluorescence intensity as a function of [18C6]/[catechol]. The fluorescence intensity in Figure 4c is normalized with that at $[18C6]_0/[catechol]_0 = 0$ solution. The fluorescence intensity of catechol increases up to $[18C6]_0/[catechol]_0 = 9.0$.

3.2.2. Fluorescence Lifetime Measurement. Figure 5b shows the decay profile of emission of catechol in cyclohexane solution

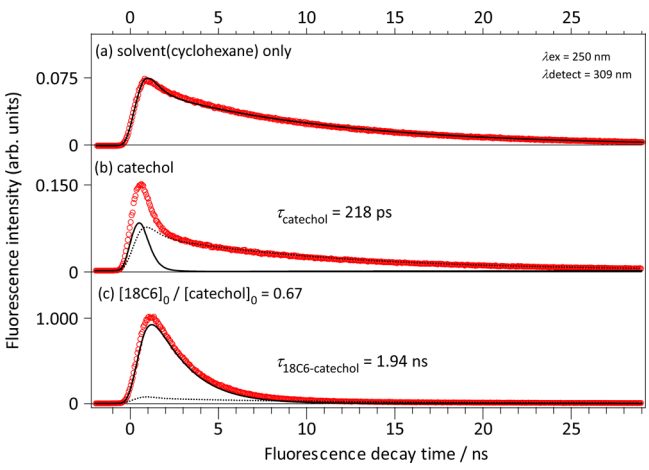

Figure 5. Fluorescence decay curves of (a) cyclohexane solvent, (b) catechol, and (c) 18C6/catechol mixture in cyclohexane solution at $[catechol]_0/[18C6]_0 = 0.67$ (red circles). The black dashed curves in parts b and c are decay profiles of cyclohexane solvent only. The intensities are normalized so that the fluorescence intensity of part c is unity. The black solid curves are decay profiles of catechol obtained by subtracting the fluorescence decay of solvent from the total decay curve. The excitation wavelength is 250 nm, and the fluorescence is detected at 309 nm.

at $[catechol]_0 = 5.3 \times 10^{-5}$ mol/L (red circles) excited at 250 nm. The decay profile shows a double exponential decay with the time constant of the fast (solid line) and slow (dashed line) components to be 218 ps and 10 ns, respectively. To investigate the reason for the double exponential decay, we measured the emission of cyclohexane itself, as shown in Figure 5a. The time profile of Figure 5a shows a single exponential decay with a lifetime of 10 ns. Thus, the slow component of the decay curve of Figure 5b is attributed to the emission of cyclohexane. However,

dx.doi.org/10.1021/jp508619f | J. Phys. Chem. B XXXX, XXX, XXX−XXX

cyclohexane does not have a chromophore which absorbs 250 nm light; the emission may be attributed to some impurity. For the fast component of Figure 5b, the time constant of 218 ps is much shorter than the excitation laser pulse width of 1.2 ns, so this value gives only an upper limit of the measurable lifetime of catechol in cyclohexane solution. As was described above, the fluorescence lifetime of gas phase catechol was reported to be 7.0 ps, and the fluorescence lifetime in cyclohexane solution may not be so different from the gas phase value. Figure 5c shows the fluorescence decay curve of 18C6/catechol mixture in cyclohexane solution measured at a $[18C6]_0/[catechol]_0$ ratio of 0.67. Deconvolution of the decay curves with the laser time profile gives a lifetime of 1.94 ns. This lifetime is attributed to the 18C6−catechol 1:1 complex formed in solution. As seen in Figure 5c, the contribution of emission of impurity in cyclohexane (dotted curve) is negligibly small. Thus, the fluorescence quantum yield of catechol dramatically increases through the complexation with 18C6 even in solution.

3.2.3. Equilibrium Constants of the 18C6 + Catechol ⇄ 18C6−Catechol Reaction in Solution. From the fluorescence intensity as a function of $[18C6]_0/[catechol]_0$ in Figure 4c, we obtain the equilibrium constant of the 18C6 + catechol ⇄ 18C6−catechol reaction in cyclohexane at room temperature. The equilibrium constant K of this reaction is expressed by concentrations of catechol, 18C6, and 18C6−catechol complex under the equilibrium condition. By employing the formation probability (α) of the 1:1 complex ($0 < \alpha < 1$), the equilibrium constant K is expressed as

$$K = \frac{[18C6{-}catechol]}{[catechol][18C6]} = \frac{\alpha[18C6]_0}{([catechol]_0 - \alpha[18C6]_0)\{(1-\alpha)[18C6]_0\}} \quad (1)$$

where [18C6−catechol] is the concentration of the 18C6−catechol complex under the equilibrium condition. In the experiment, the fluorescence of catechol monomer and 18C6−catechol complex cannot be detected separately from each other (Figure 4b). We measure the total fluorescence intensity (F), which is composed of catechol (F_1) and the 18C6−catechol complex (F_2), as a function of the ratio $[18C6]_0/[catechol]_0$ in Figure 4c.

By using the fluorescence detection efficiency of our apparatus, A, and fluorescence quantum yields, $\phi_{catechol}$ and $\phi_{18C6-catechol}$, F_1 and F_2 can be written as

$$F_1 = A[catechol]\phi_{catechol} = A([catechol]_0 - \alpha[18C6]_0)\phi_{catechol} \quad (2a)$$

$$F_2 = A[18C6{-}catechol]\phi_{18C6-catechol} = A(\alpha[18C6]_0)\phi_{18C6-catechol} \quad (2b)$$

In Figure 4c, we plotted the normalized fluorescence intensity R

$$R = \frac{F_1 + F_2}{F_1([18C6]_0 = 0)} = 1 + \frac{\alpha\phi_{18C6-catechol}}{\phi_{catechol}}\frac{[18C6]_0}{[catechol]_0} \quad (3)$$

as a function of $[18C6]_0/[catechol]_0$.

Hence, the normalized fluorescence intensity R will be proportional to $[18C6]_0/[catechol]_0$. As seen in Figure 4c, this condition is satisfied in the range of $0 < [18C6]_0/[catechol]_0 < 2.0$. We obtained the slope as

$$\frac{\alpha\phi_{18C6-catechol}}{\phi_{catechol}} = 5.5 \quad (4)$$

by a linear fitting of the plots. The ratio of the fluorescence quantum yield, $\phi_{18C6-catechol}/\phi_{catechol}$, can be obtained by the fluorescence lifetime of catechol and the 18C6−catechol complex in solution. The fluorescence lifetime of the 18C6−catechol complex in cyclohexane solution was obtained to be 1.94 ns. We assumed that the lifetime of catechol monomer in cyclohexane is the same as that of gas phase (7 ps). By using this assumption, α was estimated to be 2.0×10^{-2}. Finally, under the condition that the concentration of the 18C6−catechol complex was much lower than that of catechol, eq 1 can be simplified as

$$K = \frac{\alpha}{[catechol]_0} \quad (5)$$

Since the initial catechol concentration was $[catechol]_0 = 1.0 \times 10^{-4}$ mol/L, the equilibrium constant K was calculated to be 2.0×10^2 L/mol ($\log K = 2.3$). We compare this value with the other reaction involving 18C6, such as 18C6 + M^{n+} ⇄ 18C6−M^{n+}. The equilibrium constant of this reaction was reported to be $\log K = 2.34$ for M = Li in acetonitrile solution at 300 K,[32] 2.31 for Na^+ in methanol at 298 K,[33] 2.42 for Hg^{2+} in water at 298 K,[34] and 2.44 for Nd^{3+} in methanol at 298 K.[35] For the molecular cation PhN_2^+ in methanol, $\log K = 2.37$ at 298 K.[36] Thus, the equilibrium constant of 18C6−catechol is comparable with them, indicating that 18C6 efficiently captures catechol in solution.

4. DISCUSSION

4.1. Structure of the 18C6−Catechol 1:1 Complex. As seen in Figure 1b, there are three stable isomers (isomers **I**, **II**, and **III**) for the 18C6−catechol 1:1 complex in the gas phase. Figure 6 shows the calculated lowest energy structures of the

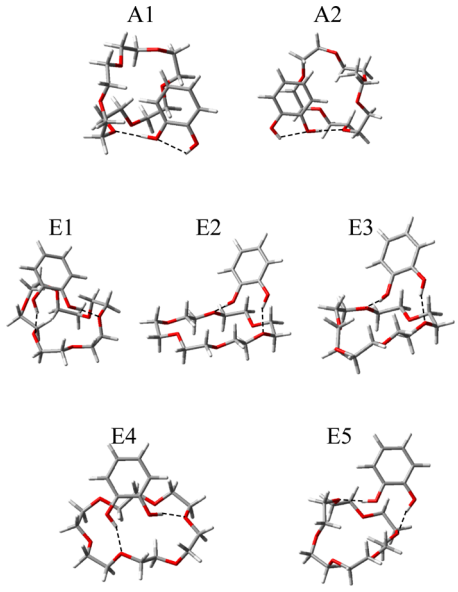

Figure 6. Lowest energy stable structures of 18C6−catechol isomers within the energy of 10 kJ/mol at the ωB97X-D/6-31++G** calculation level.

18C6−catechol 1:1 complex within the energy of 10 kJ/mol. In this energy range, seven isomers were obtained, and they can be classified into two groups, **Type-1** and **Type-2**, based on the

dx.doi.org/10.1021/jp508619f | J. Phys. Chem. B XXXX, XXX, XXX−XXX

Table 2. Relative Energies of the Stable Isomers of 18C6−Catechol Compared to the Most Stable One (A1), Dihedral Angles of C1−C2−[a]O−H3 and C2−C4−[b]O−H5, Calculated Frequencies of the OH Stretching Vibration, and Calculated Vertical Transition Energies of the S_1 ($^1\pi\pi^*$) and S_2 States with Respect to the S_0 Ground State with the Oscillator Strengths from the S_0 State (in Parentheses) of Bare Catechol, Catechol−H_2O, and 18C6−Catechol (Isomers A1, A2, and E1−E5)[a]

		dihedral angle (deg)			energy[c] (eV)	
	relative energy (kJ/mol)	[a]OH	[b]OH	OH stretching frequency[b] (cm^{-1})	S_1 ($^1\pi\pi^*$)	S_2
bare catechol		∼180	∼180	3612 ([a]OH), 3672([b]OH)	4.4256 (0.0507)	4.6820 (0.0004)
catechol−H_2O		∼180	∼180	3599 ([a]OH), 3446 ([b]OH)	4.3937 (0.0531)	4.5446 (0.0005)
A1	0	179.4	178.6	3584, 3311	4.3467 (0.0422)	4.8095 (0.0020)
A2	0.92	178.9	163.5	3584, 3325	4.3931 (0.0359)	4.8912 (0.0025)
E1	3.94	151.0	159.5	3429, 3372	4.3196 (0.0513)	5.0403 (0.0086)
E2	7.45	164.8	149.4	3396, 3386	4.3185 (0.0669)	4.8721 (0.0047)
E3	8.12	162.4	151.5	3391, 3331	4.3186 (0.0685)	4.8353 (0.0041)
E4	8.66	169.6	139.5	3390, 3404	4.3541 (0.0554)	4.9928 (0.0181)
E5	9.25	162.7	146.4	3381, 3386	4.3201 (0.0657)	4.8690 (0.0051)

[a]All calculations were performed at the level of ωB97X-D/6-31++G**. [b]All calculated OH stretching frequencies are scaled by 0.9325 so as to reproduce the observed values of catechol monomer. [c]All energies of state are scaled by 0.8598 so as to reproduce the observed S_1−S_0 electronic transition of catechol monomer.

H-bond pattern. The relative energies, the dihedral angles of the two OH groups of catechol, the OH stretching frequencies, the energies of the S_1 and S_2 states relative to the S_0 state, and the oscillator strengths of the S_1−S_0 and S_2−S_0 transitions are also listed in Table 2. **Type-1** and **Type-2** groups can be described as follows:

Type-1 (**A1** and **A2**): Catechol preserves the [a]O−H···[b]O intra-H-bond, and [b]O−H forms the inter-H-bond with an oxygen atom of 18C6. This is a similar structure with that of the catechol−H_2O 1:1 complex.[3,6] Structure **A1** is the most stable among the seven isomers, and **A2** has almost the same energy.

Type-2 (**E1**−**E5**): In these isomers, the [a]O−H···[b]O intra-H-bond is broken. Two OH groups of catechol are twisted out of the benzene plane on the same side by 20−30°, and they are independently H-bonded to oxygen atoms of 18C6. **Type-2** isomers are higher in the total energy than **Type-1** isomers by more than ∼4 kJ/mol at the ωB97X-D/6-31++G** level calculation.

Figure 2e shows the calculated IR spectra of **Type-1** (**A1**, **A2**) and **Type-2** (**E1**−**E5**) isomers. The calculated IR spectra of **Type-2** structures show very similar IR patterns with the observed ones of isomers **I** and **II**. In the spectra of **E1**−**E5**, two H-bonded OH bands appear in the 3350−3450 cm^{-1} region. For **E1** and **E3** isomers, the two OH bands are largely separated, while the two OH stretching bands are almost overlapped for **E2**, **E4**, and **E5**. Thus, isomer **I** can be assigned either to **E1** or to **E3**, and isomer **II** either to **E2**, to **E4**, or to **E5**. As seen in Table 2, **E1** is 4.2 kJ/mol more stable than **E3**, so isomer **I** can be assigned to **E1**. It is not possible to assign isomer **II** only on the basis of the total energy, because **E2**, **E4**, and **E5** have similar energies. Then, we tried to attribute the structure of isomer **II** on the basis of the S_1−S_0 transition energy. Figure 1d shows the position of the S_1−S_0 transition of **E1**−**E5**. As mentioned above, isomer **I** is attributed to **E1**. Isomer **II** shows the band origin on the blue side of band **I** with the interval of 318 cm^{-1}. As seen in Figure 1d, only isomer **E4** shows the S_1−S_0 transition on the blue side of **E1** with a large separation of ∼280 cm^{-1}. Hence, isomer **II** can be assigned to **E4**. The IR−UV spectrum of isomer **III** (Figure 2d) shows two bands at 3281 and 3507 cm^{-1}. This spectral feature is quite similar to that of **A1** and **A2**; for **Type-1** isomers, the inter-H-bonded OH ([b]OH) appears around 3300 cm^{-1}, and the band of the intra-H-bonded [a]OH appears at 3584 cm^{-1}. Therefore, isomer **III** can be assigned either to **A1** or to **A2**. Isomer **A1** is more stable than **A2** by 0.92 kJ/mol. In the LIF spectrum of the 18C6−catechol complex (Figure 1b), band **III** is located between bands **I** and **II**, which are assigned to **E1** and **E4**. The S_1−S_0 transition of **A1** is predicted to exist between **E1** and **E4**, as seen in Figure 1d. Therefore, we finally conclude that isomer **III** is ascribed to **A1**.

4.2. The Elongation of the S_1 Lifetime in 18C6−Catechol in the Gas Phase. We found that the S_1 lifetime of the **Type-2** structure of the 18C6−catechol complex (10.3 ns) is ∼1400 times longer than that of catechol monomer (7 ps) and ∼5 times longer than that of the catechol−H_2O complex (2.0 ns). Here we discuss the reason for the anomalous elongation of the S_1 lifetime of the 18C6−catechol complex relative to bare catechol and catechol−H_2O. As was mentioned in the Introduction, the short S_1 lifetime of catechol monomer is attributed to the fast internal conversion to the S_2 ($^1\pi\sigma^*$) state due to a small S_1 ($^1\pi\pi^*$)−S_2 ($^1\pi\sigma^*$) energy gap compared to other molecules.[9,11] Thus, the drastic elongation of the lifetime in the complex indicates an increase of the S_1−S_2 energy gap compared to bare catechol. We calculated the S_1 and S_2 energies of catechol and complexes by TD-DFT calculation with a fixed geometry of S_0, and the results are listed in Table 2. In the Supporting Information (Figure S1), the σ* orbital of catechol and the catechol−H_2O complex is shown. As seen in the table, in catechol monomer, the energy gap between S_1 ($^1\pi\pi^*$) and S_2 ($^1\pi\sigma^*$) is 0.25 eV in catechol and 0.15 eV in the catechol−H_2O 1:1 complex. This result seems to contradict with the experimental result that catechol−H_2O shows a longer S_1 lifetime than catechol monomer. Since the difference of the S_1−S_2 energy gap is rather small, this contradiction can be solved by higher-level calculations including zero-point energy correction. This situation is very similar to the relationship between phenol and the phenol−H_2O complex with S_1 lifetimes of 2 and 15 ns, respectively.[14−16] On the other hand, in the case of the 18C6−catechol complex, the S_2 state is located at more than 0.5 eV higher than the S_1 state for all the 18C6−catechol isomers (**I**−**III**), as seen in Table 2. In addition, the S_2 state of these isomers has mainly the $^1\pi\pi^*$ character because the oscillator strengths of the S_2−S_0 transition of the 18C6−catechol complex (∼0.008) are much larger than those of catechol and catechol−H_2O (∼0.0005). In the Supporting Information (S1), we also show the molecular orbitals involved in the S_2 state for 18C6−catechol (isomers **E1** and **E4**). We performed the TD-DFT

dx.doi.org/10.1021/jp508619f | J. Phys. Chem. B XXXX, XXX, XXX−XXX

calculations up to the S_4 states of the 18C6−catechol complex, but the $^1\pi\sigma^*$ state could not be found in these excited states. Therefore, the energy gap between the $^1\pi\pi^*$ and $^1\pi\sigma^*$ states will be larger than ∼0.5 eV for the 18C6−catechol complex, which is substantially larger than that of catechol monomer (0.25 eV). These results suggest that the $S_1(^1\pi\pi^*) \rightarrow {}^1\pi\sigma^*$ nonradiative process of catechol is prohibited upon the H-bonding with 18C6.

CONCLUSION

We investigated the structure of the 18C6−catechol complex and the effect of the complex formation on the S_1 dynamics of catechol by employing supersonic expansion/laser spectroscopic methods and theoretical calculation. We found that catechol forms three types of 1:1 complexes with 18C6 (isomers **I**−**III**). On the basis of the IR spectra and the position of the S_1−S_0 transition, isomers **I**−**III** are attributed to structures **E1**, **E4**, and **A1**, respectively. Two of the three 18C6−catechol isomers (isomers **I** and **II**) break the intramolecular H-bond between the ^{a}OH and ^{b}OH groups and form two intermolecular H-bonds with oxygen atoms of 18C6. The other isomer (isomer **III**) keeps the intramolecular H-bond, and the catechol and 18C6 components are bonded through one intermolecular H-bond. We determined the S_1 ($^1\pi\pi^*$) lifetime of bare catechol, catechol−H_2O, and 18C6−catechol. Similar to the case of phenol, the complex formation of catechol with H_2O elongates the lifetime from 7.0 ps (bare catechol) to 2.0 ns (catechol−H_2O). The lifetime is further elongated in the 18C6−catechol complex (10.3 ns). TD-DFT calculations suggest that the $^1\pi\sigma^*$ state substantially increases in energy in the 18C6−catechol complex compared to bare catechol and catechol−H_2O and the $S_1(^1\pi\pi^*) \rightarrow {}^1\pi\sigma^*$ nonradiative process is prohibited in the 18C6−catechol complex. We also observed the absorption and fluorescence spectra of catechol in cyclohexane solution at room temperature. The fluorescence intensity of catechol becomes stronger and stronger with increasing concentration of 18C6 in solution due to the formation of the 18C6−catechol complex, which has a higher fluorescence quantum yield than that of catechol monomer. We estimated the equilibrium constant for the 1:1 complex formation to be $K = 2.0 \times 10^2$ L/mol from the dependence of the catechol fluorescence intensity on the 18C6 concentration. This value is comparable to those for alkali metal ions, suggesting that 18C6 can effectively capture catechol in solution. On the basis of this efficient complex formation with a great ability of the fluorescence enhancement, 18C6 can be used as a highly sensitive sensor for catechol derivatives in solution.

ASSOCIATED CONTENT

Supporting Information

Figure 1S showing (a) the π^* and σ^* molecular orbitals of bare catechol, (b) the π^* and σ^* molecular orbitals of catechol−H_2O, and (c) the π^* orbital and the orbitals which are involved in the S_2 state for 18C6−catechol (isomers **E1** and **E4**). This material is available free of charge via the Internet at http://pubs.acs.org.

AUTHOR INFORMATION

Corresponding Author

*E-mail: tebata@hiroshima-u.ac.jp.

Notes

The authors declare no competing financial interest.

ACKNOWLEDGMENTS

The authors thank Prof. M. Abe at Hiroshima University for his kind offer to use the HORIBA Tem Pro1 for the measurement of the florescence lifetime in solution. T.E. acknowledges Japan Society for the Promotion (JSPS) for the support through a Grand-in-Aid project (No. 25410017).

REFERENCES

(1) Dunn, T. M.; Tembreull, R.; Lubman, D. M. Free-Jet Spectra and Structure of *o*-, *m*- and *p*-Dihydroxybenzene. *Chem. Phys. Lett.* **1985**, *121*, 453−457.
(2) Bürgi, T.; Leutwyler, S. O-H Torsional Vibration in the S_0 and S_1 States of Catechol. *J. Chem. Phys.* **1994**, *101*, 8418−8429.
(3) Gerhards, M.; Perl, W.; Schumm, S.; Henrichs, U.; Jacoby, C.; Kleinermanns, K. Structure and Vibrations of Catechol and CatecholH_2O(D_2O) in the S_0 and S_1 State. *J. Chem. Phys.* **1996**, *104*, 9362−9375.
(4) Gerhards, M.; Perl, W.; Schumm, S.; Henrichs, U.; Jacoby, C.; Kleinermanns, K. Structure and Vibrations of Catechol(Methanol)$_1$ in the S_0 and S_1 State. *J. Chem. Phys.* **1996**, *106*, 878−884.
(5) Gerhards, M.; Schumm, S.; Unterberg, C.; Kleinermanns, K. Structure and Vibrations of Catechol in the S_1 and Ionic Ground State. *Chem. Phys. Lett.* **1998**, *294*, 65−70.
(6) Gerhards, M.; Unterberg, C.; Kleinermanns, K. Structure of Catechol$(H_2O)_{1,3}$ Clusters in the S_0 and D_0 states. *Phys. Chem. Chem. Phys.* **2000**, *2*, 5538−5544.
(7) Kjaergaard, H. G.; Howard, D. L.; Schofield, D. P.; Robinson, T. W.; Ishiuchi, S.; Fujii, M. OH- and CH-Stretching Overtone Spectra of Catechol. *J. Phys. Chem. A* **2002**, *106*, 258−266.
(8) Ahn, D.; Jeon, I.; Jang, S.; Park, S.; Lee, S.; Cheong, W. Hydrogen Bonding in Aromatic Alcohol-Water Clusters: A Brief Review. *Bull. Korean Chem. Soc.* **2003**, *24*, 695−702.
(9) Livingstone, R. A.; Tompson, J. O. F.; Iljina, M.; Donaldson, R. J.; Sussman, B. J.; Paterson, M. J.; Townsend, D. Time-Resolve Photoelectron Imaging of Excited State Relaxation Dynamics in Phenol, Catechol, Resorcinol and Hydroquinone. *J. Chem. Phys.* **2012**, *137*, 184304.
(10) King, G. A.; Oliver, T. A. A.; Dixon, R. N.; Ashfold, M. N. R. Vibrational Energy Redistribution in Catechol during Ultraviolet Photolysis. *Phys. Chem. Chem. Phys.* **2012**, *14*, 3338−3345.
(11) Chatterley, A. S.; Young, J. D.; Townsend, D.; Żurek, J. M.; Paterson, M. J.; Roberts, G. M.; Stavros, V. G. Manipulating Dynamics with Chemical Structure: Probing Vibrationally-Enhanced Tunneling in Photoexcited Catechol. *Phys. Chem. Chem. Phys.* **2013**, *15*, 6879−6892.
(12) Weiler, M.; Miyazaki, M.; Féraud, G.; Ishiuchi, S.; Dedonder, C.; Jouvet, C.; Fujii, M. Unusual Behavior in the First Excited State Lifetime of Catechol. *J. Phys. Chem. Lett.* **2013**, *4*, 3819−3823.
(13) Young, J. D.; Staniforth, M.; Chatterley, A. S.; Paterson, M. J.; Roberts, G. M.; Stavros, V. G. Relaxation Dynamics of Photoexcited Resorcinol: Internal Conversion Versus H Atom Tunnelling. *Phys. Chem. Chem. Phys.* **2014**, *16*, 550−562.
(14) Lipert, R. J.; Bermudez, G.; Colson, S. D. Pathways of SI Decay in Phenol, Indoles, and Water Complexes of Phenol and Indole a Free Jet Expansion. *J. Phys. Chem.* **1988**, *92*, 3801−3805.
(15) Sobolewski, A. L.; Domcke, W. Photoinduced Electron and Proton Transfer in Phenol and Its Clusters with Water and Ammonia. *J. Phys. Chem. A* **2001**, *105*, 9275−9283.
(16) Sobolewski, A. L.; Domcke, W.; Dedonder-Lardeux, C.; Jouvet, C. Excited-State Hydrogen Detachment and Hydrogen Transfer Driven by Repulsive $^1\pi\sigma^*$ States: A New Paradigm for Nonradiative Decay in Aromatic Biomolecules. *Phys. Chem. Chem. Phys.* **2002**, *4*, 1093−1100.
(17) Nix, M. G. D.; Devine, A. L.; Cronin, B.; Dixon, R. N.; Ashfold, M. N. R. High Resolution Photofragment Translational Spectroscopy Studies of the Near Ultraviolet Photolysis of Phenol. *J. Chem. Phys.* **2006**, *125*, 133318.
(18) Vieuxmarie, O. P. J.; Lan, Z.; Sobolewski, A. L.; Domcke, W. Ab initio Characterization of the Conical Intersections Involved in the Photochemistry of Phenol. *J. Chem. Phys.* **2008**, *129*, 224307.

(19) Ashfold, M. N. R.; King, G A.; Murdock, D.; Nix, M. G. D.; Oliver, T. A. A.; Sage, A. G. $\pi\sigma^*$ Excited States in Molecular Photochemistry. *Phys. Chem. Chem. Phys.* **2010**, *12*, 1218−1238.
(20) Pino, G. A.; Oldani, A. N.; Marceca, E.; Fujii, M.; Ishiuchi, S.; Miyazaki, M.; Broquier, M.; Dedonder, C.; Jouvet, C. Excited state hydrogen transfer dynamics in substituted phenols and their complexes with ammonia: $\pi\pi^*$-$\pi\sigma^*$ energy gap propensity and ortho-substitution effect. *J. Chem. Phys.* **2010**, *133*, 124313.
(21) Dixon, R. N.; Oliver, T. A. A.; Ashfold, M. N. R. Tunnelling under a Conical Intersection: Application to the Product Vibrational State Distributions in the UV Photodissociation of Phenols. *J. Chem. Phys.* **2011**, *134*, 194303.
(22) Roberts, G. M.; Chatterley, A. S.; Young, J. D.; Stavros, V. G. Direct Observation of Hydrogen Tunneling Dynamics in Photoexcited Phenol. *J. Phys. Chem. Lett.* **2012**, *3*, 348−352.
(23) Kusaka, R.; Inokuchi, Y.; Haino, T.; Ebata, T. Structures of (3n-Crown-n)−Phenol (n = 4, 5, 6, 8) Host−Guest Complexes: Formation of a Uniquely Stable Complex for n = 6 via Collective Intermolecular Interaction. *J. Phys. Chem. Lett.* **2012**, *3*, 1414−1420.
(24) Inokuchi, Y.; Kobayashi, Y.; Ito, T.; Ebata, T. Conformation of L-Tyrosine Studied by Fluorescence-Detected UV-UV and IR−UV Double-Resonance Spectroscopy. *J. Phys. Chem. A* **2007**, *111*, 3209−3215.
(25) Lipert, R. J.; Colson, S. D. Persistent Spectral Hole Burning of Molecular Clusters in a Supersonic Jet. *J. Phys. Chem.* **1989**, *93*, 3894−3896.
(26) Yamada, Y.; Mikami, N.; Ebata, T. Relaxation Dynamics of NH Stretching Vibrations of 2-Aminopyridine and its Dimer in a Supersonic Beam. *Proc. Natl. Acad. Sci. U. S. A.* **2008**, *105*, 12690−12695.
(27) Kusaka, R.; Ebata, T. Remarkable Site Difference of Vibrational Energy Relaxation in Benzene Dimer: Picosecond Time-Resolved IR−UV Pump−Probe Spectroscopy. *Angew. Chem., Int. Ed.* **2010**, *49*, 6989−6992.
(28) Kolossváry, I.; Guida, W. C. Low Mode Search. An Efficient, Automated Computational Method for Conformational Analysis: Application to Cyclic and Acyclic Alkanes and Cyclic Peptides. *J. Am. Chem. Soc.* **1996**, *118*, 5011−5019.
(29) *MacroModel*, version 9.1; Schrödinger, LLC: New York, 2005.
(30) Halgren, T. A. MMFF VII. Characterization of MMFF94, MMFF94s, and Other Widely Available Force Fields for Conformational Energies and for Intermolecular-Interaction Energies and Geometries. *J. Comput. Chem.* **1999**, *20*, 730−748.
(31) Frisch, M. J.; Trucks, G. W.; Schlegel, H. B.; Scuseria, G. E.; Robb, M. A.; Cheeseman, J. R.; Scalmani, G.; Barone, V.; Mennucci, B.; Petersson, G. A.; et al. *Gaussian 09*, revision D.01; Gaussian, Inc.: Wallingford, CT, 2009.
(32) Smetana, A. J.; Popov, A. I. Lithium-7 Nuclear Magnetic Resonance and Calorimetric Study of Lithium Crown Complexes in Various Solvents. *J. Solution Chem.* **1980**, *9*, 183−196.
(33) Lin, J. D.; Popov, A. I. Nuclear Magnetic Resonance Studies of Some Sodium Ion Complexes with Crown Ethers and [2]-Cryptands in Various Solvents. *J. Am. Chem. Soc.* **1981**, *103*, 3773−3777.
(34) Izatt, R. M.; Terry, R. E.; Haymore, B. L.; Hansen, L. D.; Dalley, N. K.; Avondet, A. G.; Christensen, J. J. Calorimetric Titration Study of the Interaction of Several Uni- and Bivalent Cations with 15-Crown-5, 18-Crown-6, and Two Isomers of Dicyclohexo-18-Crown-6 in Aqueous Solution at 25.degree.C and.mu. = 0.1. *J. Am. Chem. Soc.* **1976**, *98*, 7620−7626.
(35) Izatt, R. M.; Lamb, J. D.; Christensen, J. J.; Haymore, B. L. Anomalous Stability Sequence of Lanthanide(III) Chloride Complexes with 18-Crown-6 in Methanol. Abrupt Decrease to Zero from Gadolinium(3+) Ion to Terbium(3+) Ion. *J. Am. Chem. Soc.* **1977**, *99*, 8344−8346.
(36) Izatt, R. M.; Lamb, J. D.; Rossiter, B. E.; Izatt, N. E.; Christensen, J. J.; Haymore, B. L. Thermodynamics of Formation of 18-Crown-6 Complexes with Arenediazonium and Anilinium Salts in Methanol at 25 °C. *J. Chem. Soc., Chem. Commun.* **1978**, *9*, 386−387.

dx.doi.org/10.1021/jp508619f | *J. Phys. Chem. B* XXXX, XXX, XXX−XXX